

## Supporting Information

### An intrinsically thermogenic nanozyme for synergistic antibacterial therapy

Caixia Sun,<sup>a</sup> Wenqian Wang,<sup>b</sup> Xiaolian Sun,<sup>a,c</sup> Weihua Chu,<sup>b</sup> Jun Yang,<sup>d</sup> Yanmin Ju <sup>a,c</sup> and Jianjun Dai <sup>a,b,c,e</sup>

<sup>a</sup> College of Pharmacy, China Pharmaceutical University, Nanjing 211198, China

<sup>b</sup> College of Life Science and Technology, China Pharmaceutical University, Nanjing 211198, China

<sup>c</sup> Key Laboratory of Drug Quality Control and Pharmacovigilance (Ministry of Education), State Key Laboratory of Natural Medicine, China Pharmaceutical University, Nanjing 211198, China

<sup>d</sup> Nanjing Institute for Food and Drug Control, Nanjing 210038, China

<sup>e</sup> MOE Joint International Research Laboratory of Animal Health and Food Safety, Key Laboratory of Animal Bacteriology, Ministry of Agriculture, College of Veterinary Medicine, Nanjing Agricultural University, Nanjing, 210095 China

\* Corresponding author: E-mail: [juyanmin@cpu.edu.cn](mailto:juyanmin@cpu.edu.cn) (Prof. Yanmin Ju)

### Experimental section

**Characterizations** The morphology of samples was performed using transmission electron microscopy (FEI Tecnai T20). The shape of Fe<sub>2</sub>C@Fe<sub>3</sub>O<sub>4</sub> nanoparticles (NPs) was examined using high-resolution transmission electron microscopy (FEI Tecnai F30). The dynamic light scattering (DLS) and zeta potential of samples were determined using a Zetasizer Nano-ZS (Malvern, UK). X-ray diffraction (XRD) data were obtained on a powder X-ray diffraction (D/max-2400) with a 1.54 Å Cu K $\alpha$  source. Magnetic properties of samples were recorded with a Quantum Design PPMS 9 Tesla vibrating sample magneto meter. UV-vis absorption spectra were performed on a UV-2550 (Shimadzu) spectrophotometer. X-ray photoelectron spectroscopy was measured using PerkinElmer PHI 5600. NIR thermal camera (Fluke Ti400) was used to record temperature. High frequency induction heating equipment (SPG-06-IV) was used to apply alternating magnetic fields (AMF).

**Kinetic measurement of Fe<sub>2</sub>C@Fe<sub>3</sub>O<sub>4</sub>-PEG NPs.** The steady-state kinetic assays

were carried out at 0.5 mL NaAc reaction buffer solution containing 50  $\mu$ L Fe<sub>2</sub>C@Fe<sub>3</sub>O<sub>4</sub>-PEG solution (1.8 mM iron concentration), different concentrations of H<sub>2</sub>O<sub>2</sub> (0, 0.10, 0.20, 0.30, 0.40, 0.60, 0.80 mM) or different concentrations of TMB (0, 0.10, 0.20, 0.30, 0.40, 0.60, 0.80, 1.00 mM) as the substrate. The absorbance of all reactions were monitored at different reaction time, and the Michaelis-Menten constant was calculated using the Michaelis-Menten equation:

$$1/V = K_m/V_m \times (1/S + 1/K_m)$$

where V and V<sub>m</sub> represent the initial velocity and the maximal reaction velocity, S is the concentration of substrate.

**·OH generation by peroxidase-like activity.** The generation of ·OH from H<sub>2</sub>O<sub>2</sub> catalyzed by Fe<sub>2</sub>C@Fe<sub>3</sub>O<sub>4</sub>-PEG NPs was estimated by monitoring the appearance of 2-hydroxy terephthalic acid at 425 nm.<sup>1</sup> Four experiment groups including TA (6 mM), H<sub>2</sub>O<sub>2</sub>(10 mM)+TA, Fe<sub>2</sub>C@Fe<sub>3</sub>O<sub>4</sub>-PEG(1.8 mM)+TA, Fe<sub>2</sub>C@Fe<sub>3</sub>O<sub>4</sub>-PEG(1.8 mM)+TA+H<sub>2</sub>O<sub>2</sub> were incubated at 37 °C for 30 min, respectively. Afterwards, the fluorescence intensity was detected using a FLS920 spectrometer (Edinburgh, UK) (Ex:312 nm, Em:425 nm).

***In vitro* cytotoxicity and hemolysis assay.** The cytotoxicity of Fe<sub>2</sub>C@Fe<sub>3</sub>O<sub>4</sub>-PEG NPs was evaluated with the cancer cells (HeLa) based on MTT assay. Briefly, HeLa cells were seeded in 96-well plates at a density of 1.0 × 10<sup>4</sup>/well for 24 h (37 °C, 5% CO<sub>2</sub>) and exposed to various iron concentrations of Fe<sub>2</sub>C@Fe<sub>3</sub>O<sub>4</sub>-PEG (0, 0.1125, 0.225, 0.45, 0.50, 1.80, 3.60 mM). Then, 150  $\mu$ L MTT solution containing medium (0.5 mg mL<sup>-1</sup>) was added with further incubation for 4 h at 37 °C and 150  $\mu$ L of dimethyl sulfoxide was added to dissolve the formed crystals during the MTT assay. Finally, the absorbance values of supernatant of all samples at 490 nm were measured by a microplate spectrophotometer.

Hemolysis assay was carried out on fresh rabbit blood. Rabbit blood cells were collected by centrifuging at 3000 rpm for 10 min, washed three times using phosphate buffered saline (PBS) solution (pH 7.4) and diluted to 2% with saline. Afterwards, 50  $\mu$ L red blood cell (RBC) suspension was mixed with 0.5 mL different

iron concentrations of Fe<sub>2</sub>C@Fe<sub>3</sub>O<sub>4</sub>-PEG saline dispersions (0.50, 1.80, 3.60 mM) for further incubation at 37 °C for 3 h. The positive and negative control groups were respectively pure water and saline. Finally, the absorbances of all samples were tested at 540 nm. The ratio of hemolysis was calculated by the formula:<sup>2</sup>

$$\text{Hemolysis (\%)} = (A_S - A_N) / (A_P - A_N) \times 100\%$$

Where A<sub>S</sub> represents the absorbance values of supernatant of samples resulting from the addition of nanomaterials, A<sub>N</sub> is the absorbance values of saline and A<sub>P</sub> is the absorbance values of pure water.

**Reduced natural enzyme activity induced by heat.** Log phase's bacteria were collected and washed three times with 0.9% NaCl to remove LB medium. Then, the bacteria were stored in liquid nitrogen for 5 min and resuspended with 0.9% NaCl. The bacterial suspensions were treated with ultrasonic crusher and the glutathione reductase, adenosine triphosphatases, and isocitrate dehydrogenase were collected by low temperature centrifugation (4000 rpm, 15 min). Finally, the activities of natural enzymes were detected by glutathion reductases activity assay kit (A062-1, Nanjing Jiancheng Bioengineering Institute), Ultra-micro ATPase activity assay kit (A070-1-1, Nanjing Jiancheng Bioengineering Institute) and Isocitrate dehydrogenase cytoplasmic activity assay kit (AKCO014U, Beijing Boxbio Science & Technology Co., Ltd.).

**Morphology observation of bacteria by scanning electron microscopy (SEM).**

The morphologies of bacteria were characterized by SEM. Briefly, bacteria samples were washed three times with PBS and fixed with 2.5% glutaraldehyde at 4 °C for 8 h. The fixed samples were subsequently dehydrated in ethanol solutions (50, 70, 80, 90, 95, and 100%) for 30 min. Finally, samples were dried in a freezer and coated with gold before SEM observation.

**Evaluation of bacterial membrane structure by TEM.** To observe the inner structures of bacteria, TEM observation was employed. All treated bacterial samples were collected and fixed with 2.5% glutaraldehyde solution at 4 °C for 8 h. The samples were serially dehydrated in ethanol solutions (50, 70, 80, 90, 95, and 100%)

for 15 min after postfixed in 1% osmic acid at 4 °C for 2 h. Afterwards, the embedding medium (Epon 812 (SPI 90529-77-4)) was used to permeate these dehydrated samples. Then, the samples were embedded with paraffin at 60 °C for 48 h and ultrathin sections (about 80 nm) were obtained by a microtome (Leica UC7). Lastly, sections were dried and stained with uranylacetate for TEM observation.

**Live/dead staining observation.** After respective treatments by Fe<sub>2</sub>C@Fe<sub>3</sub>O<sub>4</sub>-PEG and/or H<sub>2</sub>O<sub>2</sub> and/or alternating magnetic field and near-infrared irradiation, the *E.coli* and *S.aureus* cells were collected by centrifuging at 3000 rpm for 3 min and stained with SYTO9 and propidium iodide for 40 min at 37 °C. The *E.coli* and *S.aureus* cells with different treatments were observed under Laser Scanning Confocal Microscope (LSM700, Carl Zeiss).

**Detection of cellular reactive oxygen species (ROS).** The *E. coli* cells which harvested by centrifuging at 3000 rpm for 3 min after respective treatments were stained with DCFH-DA (10 μM) probe for 30 min in the dark. Subsequently, the fluorescence intensity of DCF was detected by Laser Scanning Confocal Microscope (LSM700, Carl Zeiss).

**Protein leakage assay.** The protein leakage level of *E. coli* and *S.aureus* induced by different treatments was detected by BCA Protein Assay Kit (Cat#P0012, Beyotime Biotechnology). After laser irradiation, the bacterial suspension collected by centrifuging (3000 rpm, 3 min) were added into a 96-well plate and the content of protein was measured at 562 nm using a microplate reader.

**16S rRNA gene sequence.** The 16S rRNA gene of strains from infected wounds were checked by Shanghai Lingen Biotechnology Co., Ltd using the upstream primer (27F 5'-AGAGTTTGATCMTGGCTCAG-3') and the downstream primer (1492R 5'-CGGTTACCTTGTTACGACTT-3'). Sequencing results for the 16S rRNA genes were submitted to GenBank database and species identification could be accepted with homology of 98.5% and above.

**H&E staining assay.** For evaluating the safety of Fe<sub>2</sub>C@Fe<sub>3</sub>O<sub>4</sub>-PEG *in vivo*, major organs of mice (heart, liver, spleen, lung, and kidney) were conducted for H&E staining analysis.

**Statistical analysis.** All data were presented as means  $\pm$  standard deviations. A value of  $P < 0.05$  was considered significant. The Student's t-test was used to represent the statistical significance of the differences between groups.



**Figure S1.** The synthesis schematic of Fe<sub>2</sub>C@Fe<sub>3</sub>O<sub>4</sub> NPs.

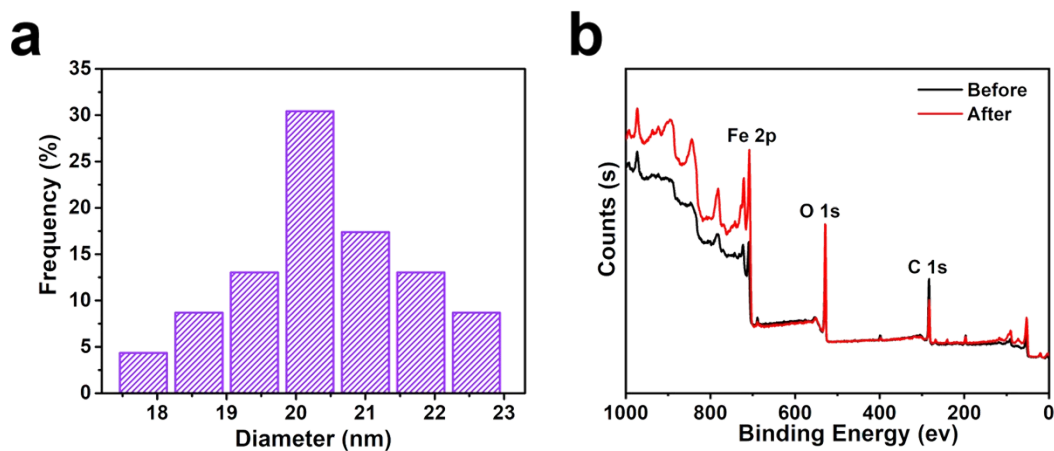


**Figure S2.** Characterizations of Fe<sub>2</sub>C@Fe<sub>3</sub>O<sub>4</sub>-PEG NPs. a) particle diameter distribution range and b) XPS survey scan before and after argon-ion bombardment of Fe<sub>2</sub>C@Fe<sub>3</sub>O<sub>4</sub> NPs.

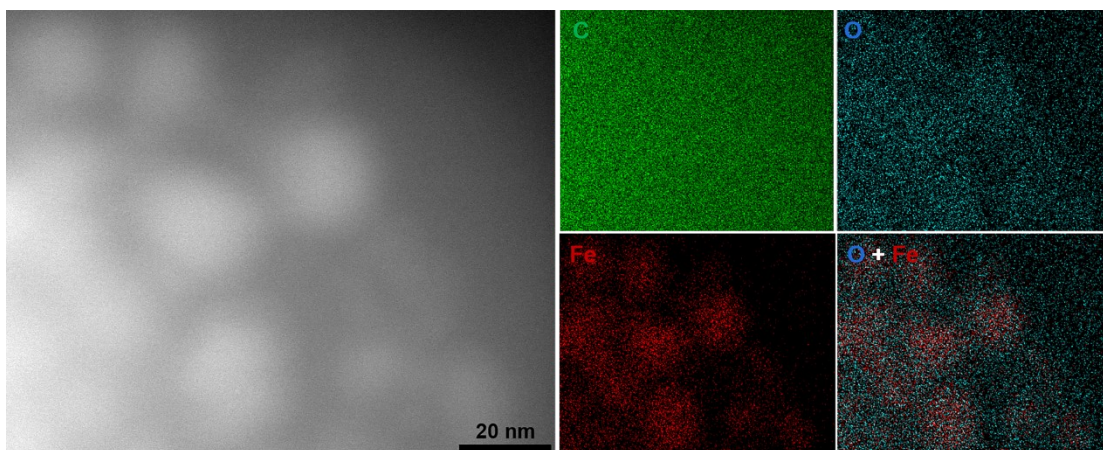


**Figure S3.** HADF-STEM and EDS elemental mapping images of Fe<sub>2</sub>C@Fe<sub>3</sub>O<sub>4</sub>-PEG NPs.

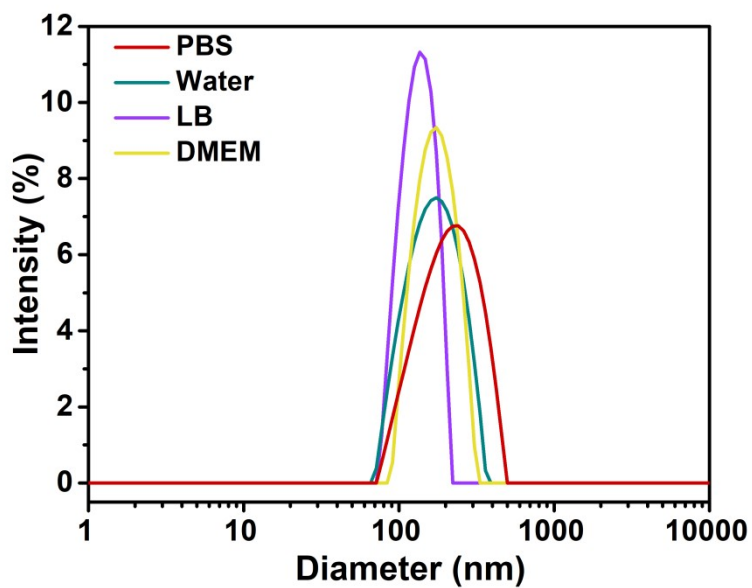


**Figure S4.** DLS of Fe<sub>2</sub>C@Fe<sub>3</sub>O<sub>4</sub>-PEG NPs in PBS, water, LB and DMEM.

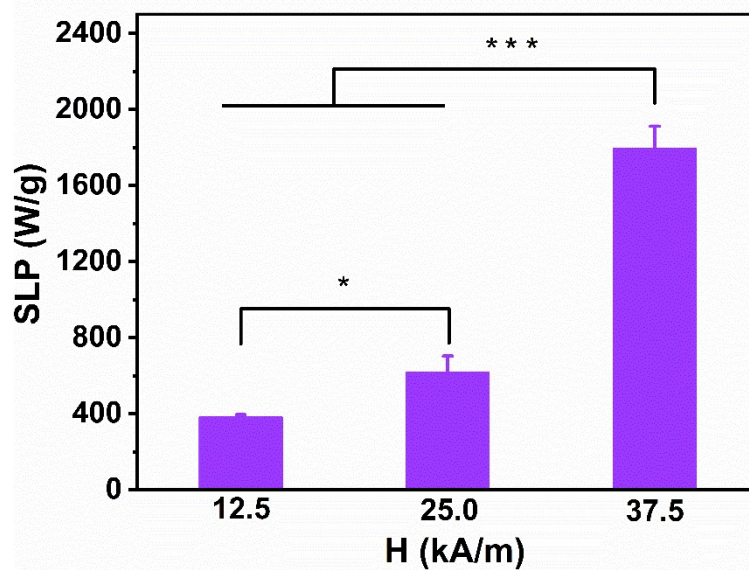


**Figure S5.** The SLP values of  $\text{Fe}_2\text{C}@Fe_3O_4$ -PEG NPs treated with different strength of AMF. Error bars represent standard error of mean and \*, \*\*, and \*\*\* indicate obvious differences at  $p < 0.05$ ,  $p < 0.01$ , and  $p < 0.001$ .

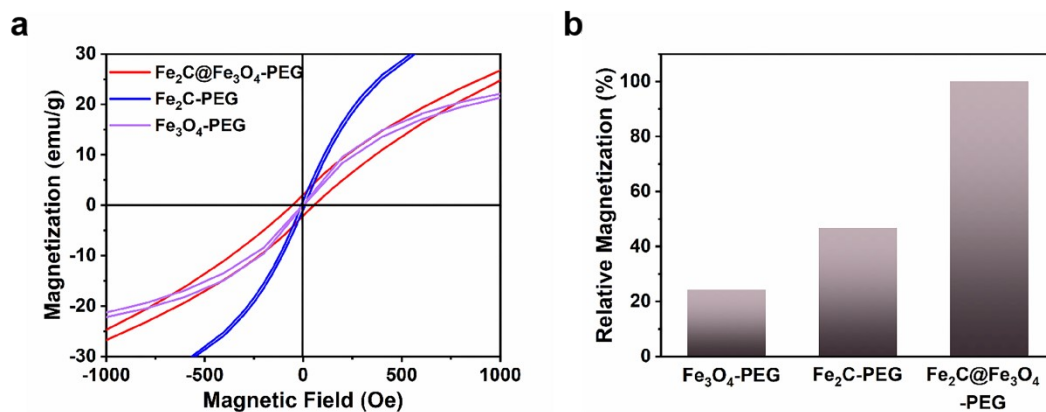


**Figure S6.** a) Field-dependent magnetization curves and b) relative magnetic energy product of  $\text{Fe}_2\text{C}@Fe_3O_4$ -PEG NPs,  $\text{Fe}_2\text{C}$ -PEG NPs and hollow  $Fe_3O_4$ -PEG NPs at room temperature (magnetic field range from -1000 Oe to 1000 Oe).

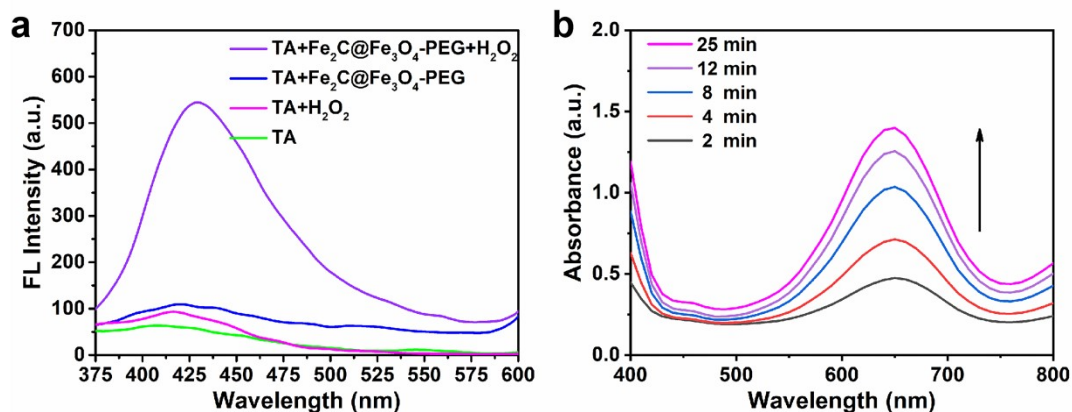


**Figure S7.** Thermal-enhanced peroxidase-like properties of Fe<sub>2</sub>C@Fe<sub>3</sub>O<sub>4</sub>-PEG NPs. a) Fluorescence spectra of different TA solutions. b) UV/vis absorption spectra of Fe<sub>2</sub>C@Fe<sub>3</sub>O<sub>4</sub>-PEG NPs co-incubated with TMB and H<sub>2</sub>O<sub>2</sub> at different time.

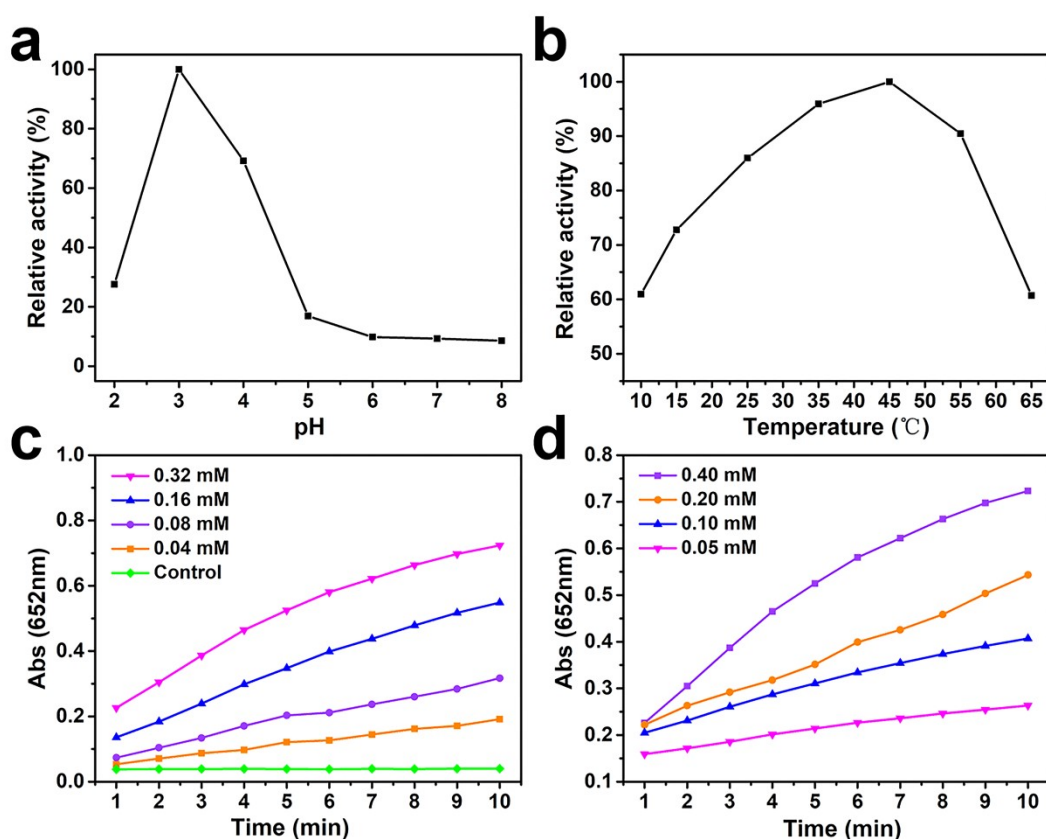


**Figure S8.** Peroxidase-like properties of Fe<sub>2</sub>C@Fe<sub>3</sub>O<sub>4</sub>-PEG NPs. a) The relative activity of peroxidase-like properties of Fe<sub>2</sub>C@Fe<sub>3</sub>O<sub>4</sub>-PEG NPs in different pH and b) temperature. Relationship between the yield of •OH and the various concentrations

of c)  $\text{Fe}_2\text{C}@\text{Fe}_3\text{O}_4\text{-PEG NPs}$  and d)  $\text{H}_2\text{O}_2$ .

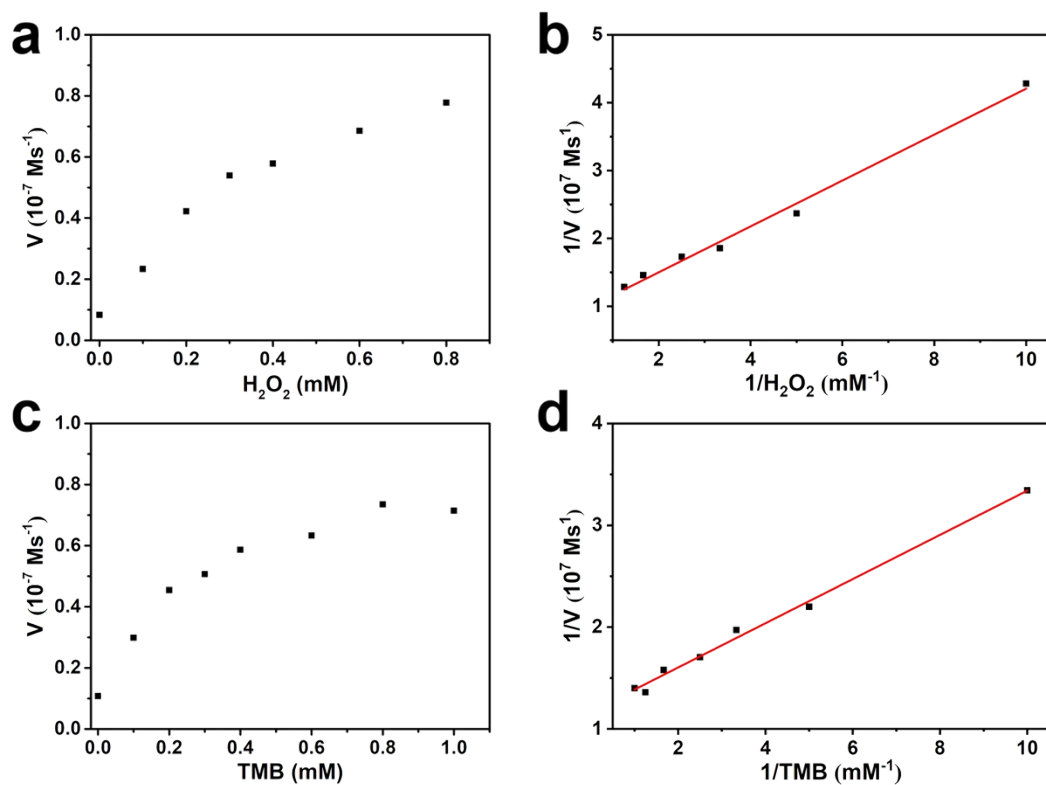


**Figure S9.** Kinetic measurement of  $\text{Fe}_2\text{C}@\text{Fe}_3\text{O}_4\text{-PEG NPs}$ . Steady-state kinetic assay of a)  $\text{Fe}_2\text{C}@\text{Fe}_3\text{O}_4\text{-PEG NPs}$  to  $\text{H}_2\text{O}_2$  substrate and b) corresponding generated double-reciprocal plot. Steady-state kinetic assay of c)  $\text{Fe}_2\text{C}@\text{Fe}_3\text{O}_4\text{-PEG NPs}$  to TMB substrate and d) corresponding generated double-reciprocal plot.

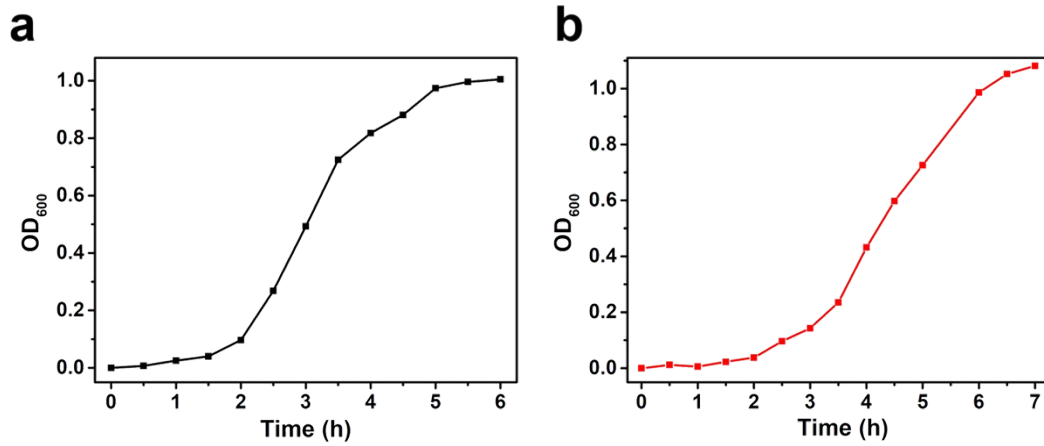


**Figure S10.** The growth curve measurement of *E. coli* and *S. aureus*.

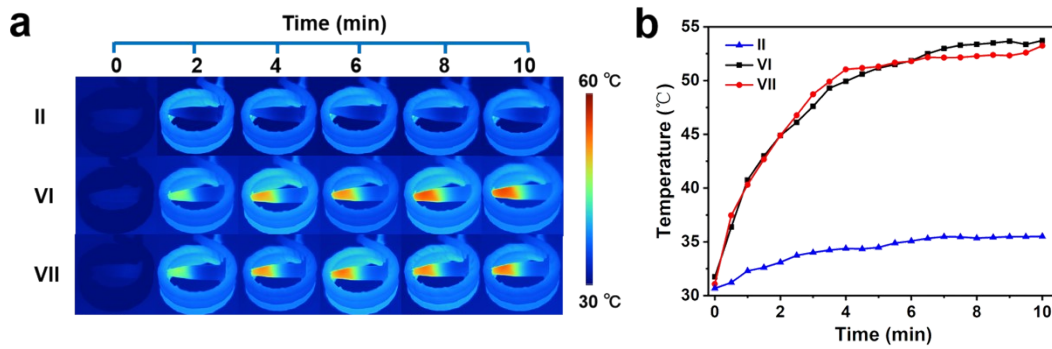


**Figure S11.** Magnetothermal effects of Fe<sub>2</sub>C@Fe<sub>3</sub>O<sub>4</sub>-PEG NPs after co-incubated with *S. aureus*. a) Infrared thermal images of *S. aureus* treated AMF. b) Quantification of temperature for different groups shown in infrared thermal images. Amongst (II) AMF, (VI) Fe<sub>2</sub>C@Fe<sub>3</sub>O<sub>4</sub>-PEG+AMF and (VII) Fe<sub>2</sub>C@Fe<sub>3</sub>O<sub>4</sub>-PEG+H<sub>2</sub>O<sub>2</sub>+AMF.

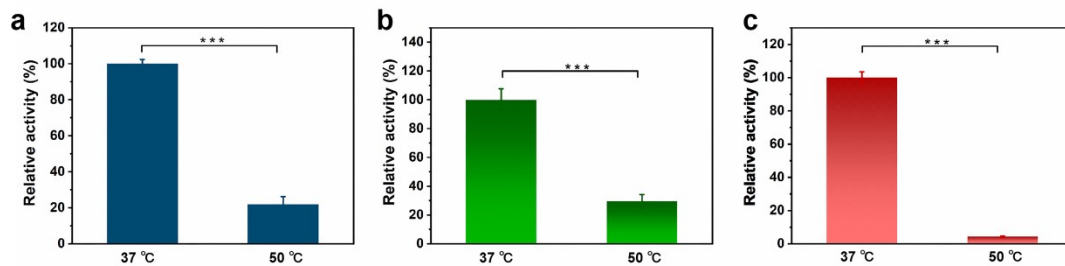


**Figure S12.** The activity of a) GR, b) ATPase and c) IDH after treatment with saline (37 °C and 50 °C).

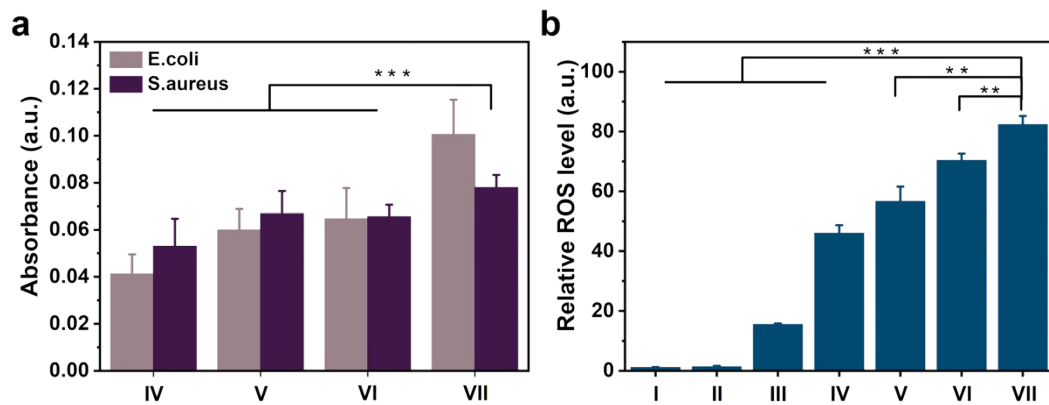


**Figure S13.** Antibacterial mechanism of  $\text{Fe}_2\text{C}@\text{Fe}_3\text{O}_4\text{-PEG}$  NPs. a) The cytoplasm leakage of bacteria checked by BCA kits. b) The green fluorescence intensity reflecting  $\bullet\text{OH}$  radical level in *E. coli* after different treatments. Error bars represent standard error of mean ( $n=3$ ) and \*, \*\*, and \*\*\* indicate obvious differences at  $p < 0.05$ ,  $p < 0.01$ , and  $p < 0.001$ .

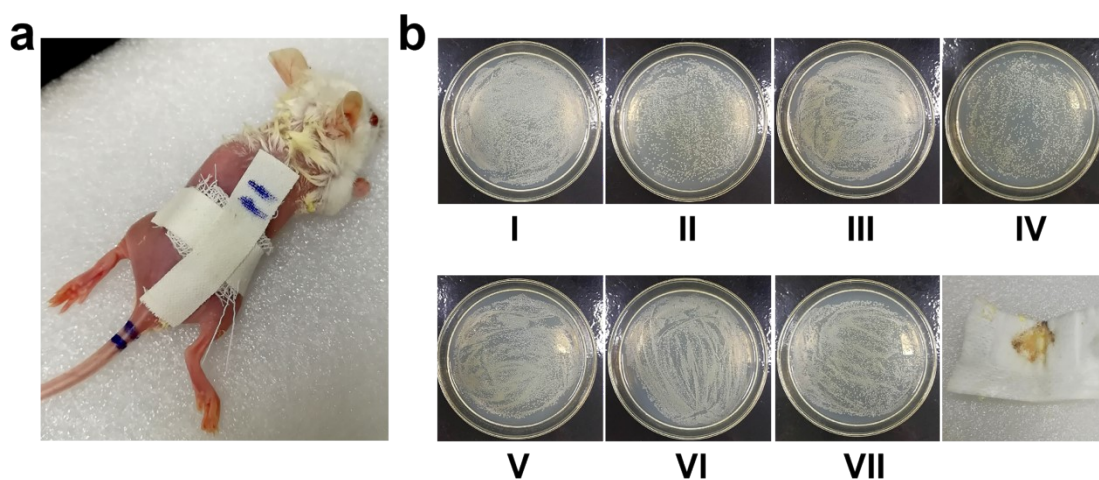


**Figure S14.** The construction of mouse model. a) The typical construction of mouse infection model. b) The plate results and pus of seven groups of mice at the infected

site one day after bacterial infection. Amongst, (I) control, (II) AMF, (III) H<sub>2</sub>O<sub>2</sub>, (IV) Fe<sub>2</sub>C@Fe<sub>3</sub>O<sub>4</sub>-PEG, (V) Fe<sub>2</sub>C@Fe<sub>3</sub>O<sub>4</sub>-PEG+H<sub>2</sub>O<sub>2</sub>, (VI) Fe<sub>2</sub>C@Fe<sub>3</sub>O<sub>4</sub>-PEG+AMF and (VII) Fe<sub>2</sub>C@Fe<sub>3</sub>O<sub>4</sub>-PEG+H<sub>2</sub>O<sub>2</sub>+AMF.

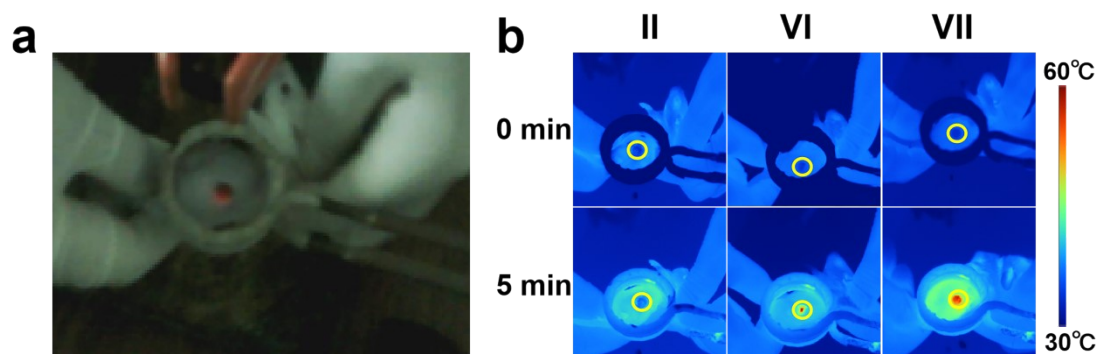


**Figure S15.** a) The operational diagram of animal experiments, infected wound (yellow circle) was fixed in alternating magnetic field. b) Infrared thermal images of infected area of mice.

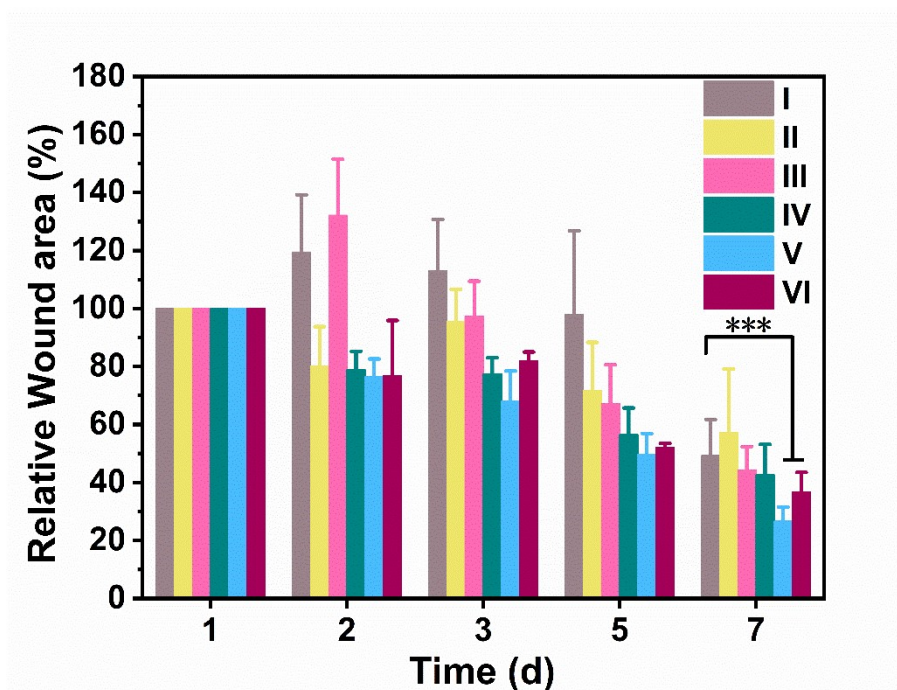


**Figure S16.** Wound healing status after different treatments. \*, \*\*, and \*\*\* indicate obvious differences at  $p < 0.05$ ,  $p < 0.01$ , and  $p < 0.001$ .

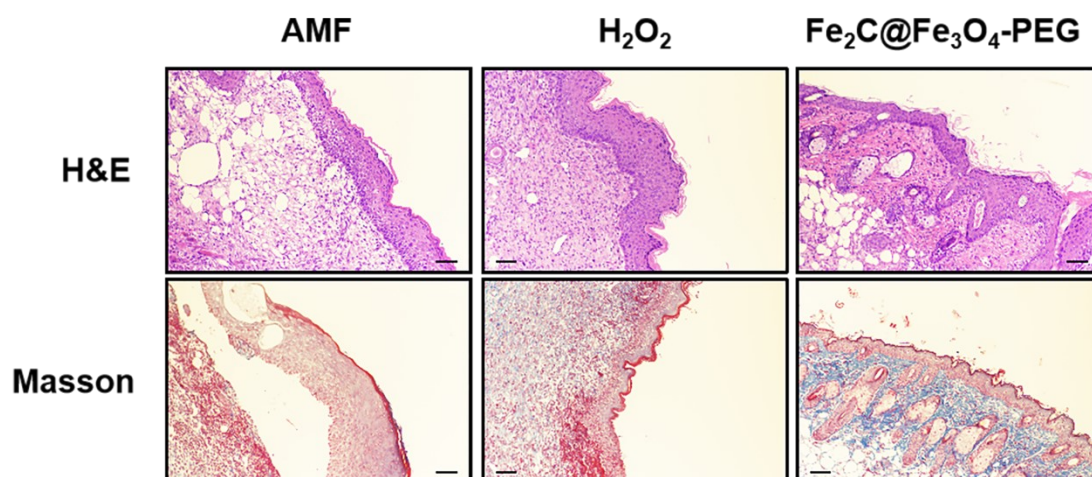


**Figure S17.** H&E staining and Masson staining of the infected skin with different treatments.

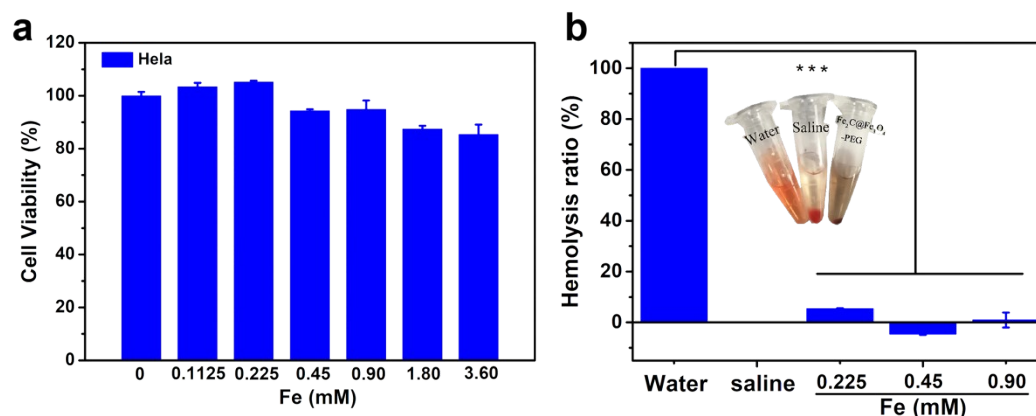


**Figure S18.** Toxicity evaluation of  $\text{Fe}_2\text{C}@Fe_3O_4\text{-PEG}$ . a) Cell viability of  $\text{Fe}_2\text{C}@Fe_3O_4\text{-PEG}$  determined by MTT cytotoxicity colorimetric assays using human cervical carcinoma (HeLa) cells. b) Hemolysis ratio of fresh rat red blood cells (RBCs) incubated with  $\text{Fe}_2\text{C}@Fe_3O_4\text{-PEG}$ . Inset: RBCs incubated with saline, water and  $\text{Fe}_2\text{C}@Fe_3O_4\text{-PEG}$ . Error bars are based on three samples and \*, \*\*, and \*\*\* indicate statistically significant differences at  $p < 0.05$ ,  $p < 0.01$ , and  $p < 0.001$ .

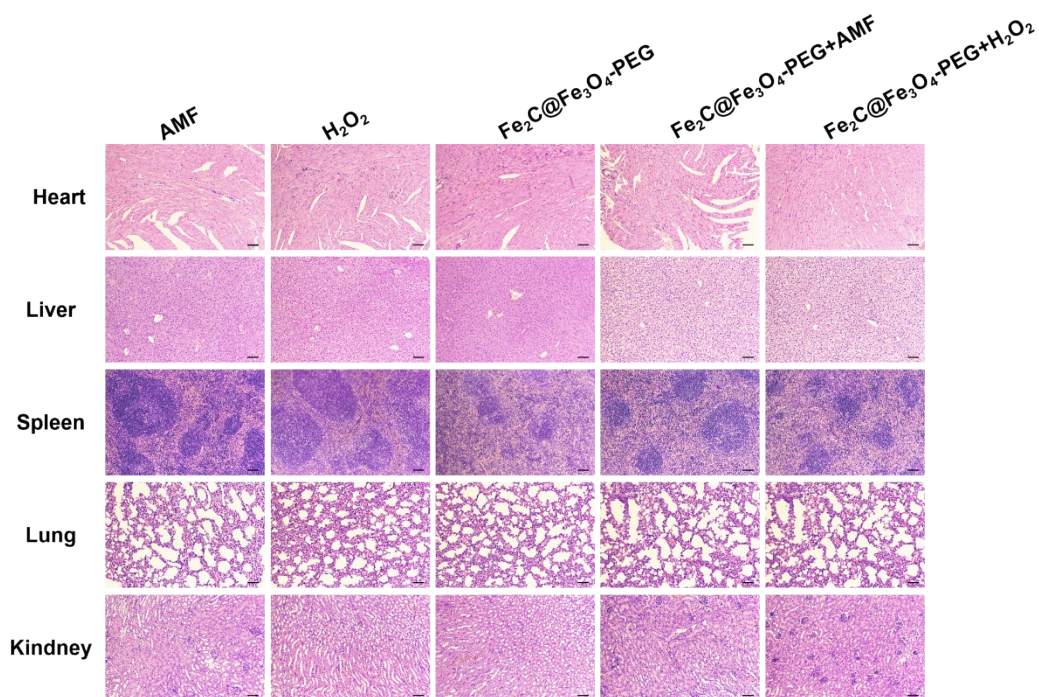


**Figure S19.** H&E staining of the heart, liver, spleen, lung, and kidney at day 7 after with different treatments (scale bar=100  $\mu$ m).

**Table S1** The colony forming unit and inhibition rate of *S.aureus* and *E.coli* with different treatment.

		Control	Fe <sub>2</sub> C@Fe <sub>3</sub> O <sub>4</sub> -PEG+H <sub>2</sub> O <sub>2</sub>	Fe <sub>2</sub> C@Fe <sub>3</sub> O <sub>4</sub> -PEG+AMF	Fe <sub>2</sub> C@Fe <sub>3</sub> O <sub>4</sub> -PEG+H <sub>2</sub> O <sub>2</sub> +AMF
<i>S.aureus</i>	Colony forming unit	5100	617	1139	89
	Bacterial inhibition rate	NA	87.9%	77.67%	98.25%
<i>E.coli</i>	Colony forming unit	403	81	81	17
	Bacterial inhibition rate	NA	79.91%	79.91%	95.79%

**Table S2.** 16S rRNA gene sequencing identification of bacterium in infected area.

GenBank accession number	Closest relative bacterium	Identity (%)
MW173230	<i>Escherichia coli</i> strain 25922	100.00

### Supplementary references

- 1 W.C. Hu, M.R. Younis, Y. Zhou, C. Wang, X.H. Xia, *Small*, 2020, **16**, e2000553.
- 2 Z. Yuan, C.C. Lin, Y. He, B.L. Tao, M.W. Chen, J.X. Zhang, P. Liu, K.H. Cai, *ACS Nano*, 2020, **14**, 3546-3562.